SUMMER INTERNSHIP REPORT(16TH MAY TO 15TH JULY 2016)

MODELING OF DYNAMIC RECRYSTALLISATION

NAME: ADITYA VENKATRAMAN

GUIDE: PROF. YUNG C. SHIN

(Donald A. and Nancy G. Roach Professor of Advanced Manufacturing)

GRADUATE MENTOR: POOJA NITIN SHAH

CONTENTS

ACKNOWLEDGEMENTS

Foremost, I would like to express my sincere gratitude to my advisor Prof. Yung Shin for agreeing to guide me through the PURE program. I would also like to thank him for his continuous support of my study and research, for his patience, motivation, enthusiasm, and immense knowledge. His guidance helped me in all the time of research. I could not have imagined having a better advisor and mentor for my internship.

Besides my advisor, I would like to thank Pooja N.Shah, for her encouragement, insightful comments, and guidance throughout my stay here at Purdue University. I hope being a graduate mentor didn't distract her too much from her graduate project.

My sincere thanks also goes to Dr. Dan Perlman, Ms.Heidi Arola, and Dr. David Janes, for offering me the summer internship opportunities as a part of the PURE program that enabled me to work on an exciting project.

INTRODUCTION AND OBJECTIVE

One of the techniques available for improving strength as well as ductility is grain refinement via severe plastic deformation (SPD). A number of SPD techniques have been used to deform materials to generate ultrafine grained (UFG) microstructure leading to enhanced physical and mechanical properties. To accumulate large enough plastic strain, multi passes are usually needed for cold rolling a flat metal piece to refine the microstructure from tens of micrometres or greater to a few hundred nanometres. The evolution of microstructure, particularly the formation of ultra-fine grained microstructure during cold rolling, has been experimentally studied for a variety of metallic materials. Examples include AA1200 (by Liu et.al.2002) and commercially pure titanium (Yang.et.al.2010).

The refinement of grains happens according to a similar pattern. As the strain increases, the thickness of the cell walls decreases and the original grains break down and become subdivided into smaller sub-grains. The dislocation cell walls evolve into grain boundaries (GBs), and ultimately an array of ultrafine grains with high-angle non-equilibrium GBs are formed. The large-strain accumulated over repetitive passes of cold rolling has been generally used as a qualitative measure to the change of microstructure.

While the aforementioned work has produced knowledge with regard to microstructure and properties of cold rolled materials, it is noted that these experimentally achieved empirical relationships of strain-microstructure cannot be simply extended to a different process or a different material, because each cold rolling condition for each material is unique and all the process parameters such as temperature and strain rate affect the resultant microstructure. Therefore, it is critical to validate predictive models based on the mechanism of grain refinement to better design and optimize a multi-pass cold rolling process for producing a desirable cold rolled microstructure.

Typical modelling efforts in the high temperature regime follow dislocation theories. These approaches are mostly based on stress-dislocation relations and kinematics of the dynamic recovery (DRV) and dynamic recrystallization (DRX). Materials whose dislocations are able to cross-slip and climb can easily rearrange into polygonal sub-grain structures and tend to display a high degree of DRV, while materials with low stacking fault energy show a much lower level of DRV. In the latter case, dislocation density rises until it reaches a critical condition, at which point new grains nucleate and grow during further straining. Some other common modelling efforts in hot forming include the development of respective constitutive equations from the experimental stress-strain curves to describe the flow response.

This report attempts to study the modelling of the DRX for multi-pass rolling process by implementation of microstructure based constitutive model in Abaqus. Some relevant results are shown regarding the validation.

THE FLOW BEHAVIOUR IN HIGH TEMPERATURE PROCESSES

The effects of temperature and strain rate are significant on the flow stress behavior of severely deformed titanium (Fig. 2). The flow stress obtained at a particular temperature is greater than those obtained at temperatures above it. The stress-strain curves exhibit moderate work hardening (WH) rate during hot compression at the lowest deformation temperature, especially at higher strain rates. In contrast, the flow stresses display slight transitional drops indicating thermal softening for deformation temperatures above 873K. It is well known that DRX takes place only after a critical strain (ε_c) has been exceeded.

Based on the variation of peak stress as a function of temperature at different strain rates, it can be seen that flow stress levels decrease with increasing deformation temperature. This can be attributed to reduced dislocation interactions leading to lower WH rate. The peak stress levels rise with increasing strain rate and decreasing temperature. Lower strain rates and higher temperatures provide longer time for energy accumulation and higher mobility at boundaries for the nucleation and growth of dynamically recrystallized grains and dislocation annihilation and hence result in lower flow stress levels.

WH rate is an important factor in the evaluation of the plastic deformation. The deformability, ductility, and toughness of materials are intimately linked to the hardening capacity. The evolution of DRV and DRX can also be analyzed by plotting the WH rate versus true strain curves as shown in Fig. 2.Generally, the WH rate decreases sharply with increasing strain according to Fig. 2. The strain for maximum softening rate (i.e., the minimum WH rate) increases with increasing strain rate and decreasing temperature. This trend can also be observed by considering the Z parameter. It is well known that the softening behavior is not pronounced at the condition of high Z (Ref 3). Therefore, decreasing the strain rate and increasing the forming temperature can lead to accelerated softening during hot compression. According to the work by Shaban and Eghbali (Ref 3) DRX can occur when the WH rate reaches zero followed by passing into the negative region, and the first cycle of DRX comes to the end when WH rate reaches to zero again with the increasing strain. The WH rate versus true strain relationship indicates that a complete cycle of DRX can be seen at the lower strain rate and/or higher deformation temperature values, while a single cycle can hardly be completed at high strain rates and/or low temperature (Fig. 2).

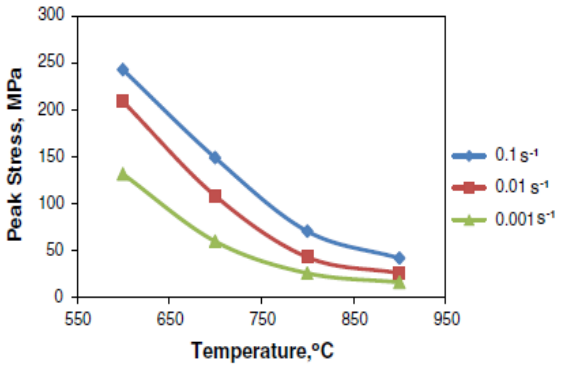

Fig.1 – Peak Stress vs T

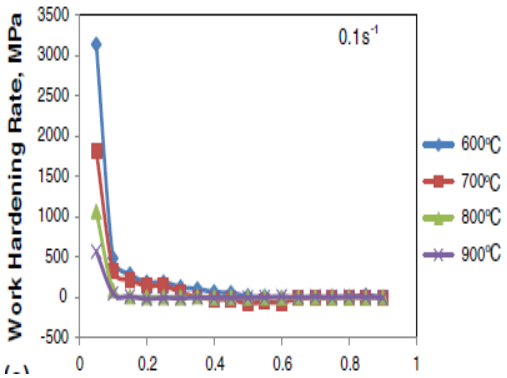

Work Hardening rate vs Strain

The general descriptive model for DRX is that the nucleation of DRX grains can start at a critical strain which is a function of initial microstructure and deformation conditions. Then, the evolution of DRX microstructure can proceed further by increasing deformation and through the formation of a necklace structure.

A strong relationship exists between True-stress strain curves and DRX.

It is well known that, due to the combined effect of WH and thermally activated softening mechanisms, most of the flow stress curves at elevated temperatures include four various stages especially at relatively low strain rates: stage I (WH stage), stage II (transition stage), stage III (softening stage) and stage IV (steady stage). These stages can be observed in Fig. 3. The WH rate overcomes the softening rate induced by DRV in stage I, and thus the stress considerably increases during initial deformation then rises at a decreased rate, followed by stage II. The competition between WH and softening induced by both DRV and DRX occurs in stage II. Usually DRX occurs only after a critical strain (ε_c) is exceeded. The critical strain (ε_c) of metallic materials was observed to be less than the strain corresponding to the peak stress (ε_p). In stage II, the flow stress still increases with a continuous decrease in rate. The stress drops sharply, which is related to dominance of DRV and DRX in stage III. Finally, the stress levels off and the plateau formation in stage IV indicates a new balance between thermal softening and WH in newly recrystallized grains.

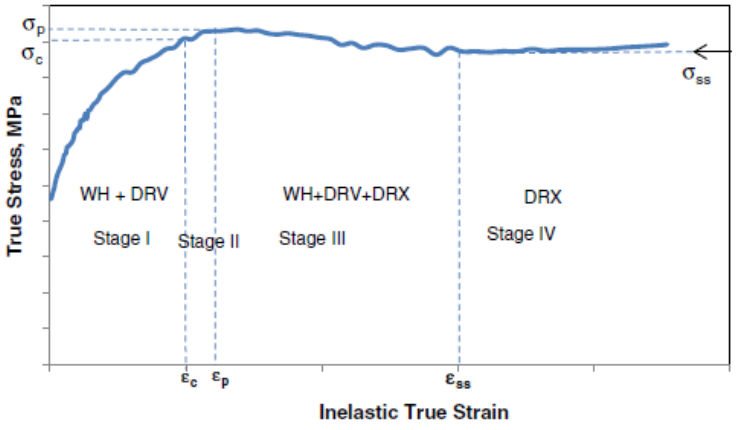

Fig.3 – Various stages in the tensile behaviour of metals

The various characteristic points exist on the curve are

$\boldsymbol{\varepsilon_c}$ = critical strain for DRX initiation

$\boldsymbol{\varepsilon_p}$ = strain at peak stress

$\boldsymbol{\varepsilon^*}$ = strain at a maximum softening rate that can be found out at the inflection point of the curves

$\boldsymbol{\sigma_p}$ = peak stress in the stress-strain curve

$\boldsymbol{\sigma_{ss}}$ = steady-flow stress in the curve that is caused by the balancing out of the work hardening due to plastic strain and softening due to DRV and DRX.

All these values are functions of the Zener-Hollomon parameter,

$$Z = \dot{\varepsilon} * e^{\frac{Q}{RT}}$$

All the stress-strain curves exhibit three distinct stages. Work-Hardening dominates in the first stage and this causes an increase of flow stress with strain. Then the recovery due to dislocation annihilation happens and we achieve a slower increase in the rate of increase. And at a particular strain, DRX starts, and the increase in work hardening after this is minimal. It then reaches a peak at ε_p, after which, a steady state value is reached after a long declining period.

A steady-state value is a strong characteristic of lower values of strain rate and higher temperature because the rate of work hardening is slower (at lower strain rates) and also, the nucleation rates and mobility of dislocations at a higher temperature as they follow Arrhenius kinetics for diffusion across grain boundaries.

$$\dot{\varepsilon} = AF(\sigma)exp(-\frac{Q}{RT})$$

where, $F(\sigma) = \begin{cases} |\sigma|^n & \alpha|\sigma|<0.8; \\ \exp(\beta|\sigma|) & \alpha|\sigma|>1.2 \\ [\sinh(\alpha|\sigma|)]^n & \text{for all } \sigma \end{cases}$

The above form of the equations has been used to determine the material constants required, namely n and α.

- From the low-end of the stress-strain plot, we get exponent ‘n’.
- From the higher end of the stress-strain curve, we get ‘β’

To put it in a better way,

- we substitute F (σ) in the strain rate equation and determine 'n' as the inverse of the slope of the **ln (σ)- ln ($\dot{\varepsilon}$)**plot.

$$\frac{\partial \ln(\dot{\varepsilon})}{\partial \ln(\sigma)} = n, \text{ at constant T}$$

- As for the value of 'β', we get it from the inverse of the slope of the **σ-ln ($\dot{\varepsilon}$)** plot.

$$\left(\frac{\partial \ln(\dot{\varepsilon})}{\partial \sigma}\right)^{-1} = \beta$$

- The value of the activation energy, Q, can be found out from the slope of the **ln (sinh(α|σ|))-1/T plot**.

$$\frac{\partial \ln(\mathbf{sinh}(\boldsymbol{\alpha}|\boldsymbol{\sigma}|))}{\partial(\frac{\mathbf{1}}{\mathbf{T}})} = Q$$

- Now, that we have the values of α,n,Q, we can get strain rate in terms of stress (or flow stress). This gives us the relation b/w flow stress and the Zener-Hollomon parameter.
- The material constants that include critical strain and peak strain are determined as **power-law functions** of the parameter Z ;

$$\boldsymbol{\varepsilon_c, \varepsilon_p, \ \varepsilon^*, \sigma_p = f(Z)}$$

- The fraction of recrystallized material X_{DRX}, can be determined based on Avrami's based kinetics.

$$X_{DRX} = 1 - exp\{-K(Z)[\frac{\varepsilon - \varepsilon_c}{\varepsilon^p}]^m\}$$

- The strain for maximum softening rate, ε^*, are attained when the value **of θ = dσ/dε** reaches the negative peak which corresponds to a valley point of **dσ/dε versus σ** plot after the peak point of the true stress–strain curve, and this is obtained at various strain rates for a given temperature.

- The critical strain however is the inflection point in the **dσ/dε –σ** plot, plotted at various temperatures, at given strain rate that indicates onset of recrystallization.

$$\frac{\partial^2 \theta}{\partial \sigma^2} = 0 \ at \ \varepsilon = \varepsilon_c$$

<u>Constitutive equations for stage I:</u>

The flow stress data for CP Ti was obtained from the torsion tests conducted by Sheikh-Ahmad and Bailey (1995 – Ref4) for the temperature range from the ambient temperature to 750 ◦C and at shear strain rate in the range from 0.192 to 122.0 s−1. The flow stress/strain relationships for AA 1200 under varying temperatures and strain rates were provided by the Johnson-Cook type constitutive plastic model (Akbari Mousavi et al., 2010- Ref5).

For Cp-Ti, the relationship between flow-shear stress and plastic shear strain is as follows;

$$\tau = B * \gamma^n * \left(1 + C * \ln\left(\frac{\dot{\gamma}}{\gamma^0}\right)\right) * \alpha e^{\frac{\beta(Tm-T)}{Tm-Tref}}$$

For AA1200, the phenomenological model is the Johnson-Crook model (ref 6):

$$\sigma = (A + B * \varepsilon^{n}) * \left(1 + C * \ln\left(\frac{\dot{\varepsilon}}{\dot{\varepsilon}^{0}}\right)\right) * \left(1 - \left(\frac{(T - Tref)}{(Tm - Tref)}\right)^{m}\right)$$

The material constants taken from Ref7 are shown below:

Table 3
Johnson-Cook model parameters of commercially pure titanium and aluminum.

Material	A_{al} (MPa)	B_{al} (MPa)	n_{al}	C_{al}	m_{al}	T_{ref} (°C)	T_m (°C)	$\dot{\varepsilon}_o$ (s^{-1})
AA 1200	80	120	0.73	0.008	1.7	25	660	1
Material	B_{ti} (MPa)	n_{ti}	C_{ti}	α_{ti}	β_{ti}	T_{ref} (°C)	T_m (°C)	$\dot{\gamma}_o$ (s^{-1})
CP Ti	294.15	0.294	0.053	0.021	3.862	150	1668	0.192

The dislocation density-based model is briefly presented in this section and more detailed descriptions can be found from the work of Lemiale et al. (2010) – ref 8 and Estrin and Kim (2007) – ref 9. In the model, a dislocation cell structure is assumed to form during deformation, which consists of two parts, dislocation cell walls and cell interiors, and obeys a rule of mixtures. The different types of dislocation densities are distinguished in the model: the cell interior dislocation density (ρ_c) and the cell wall dislocation density (ρ_w), which is further divided into two distinct groups of statistical dislocation density (ρ_{ws}) and geometrically necessary dislocation density (ρ_{wg}). The evolutions of the dislocation densities follow different routes and are governed by the following equations:

$$\dot{\rho}_c = \alpha^* \frac{1}{\sqrt{3}b}\sqrt{\rho_{ws} + \rho_{wg}}\,\dot{\gamma}_w^r - \beta^* \frac{6}{bd(1-f)^{1/3}}\dot{\gamma}_c^r \qquad - k_o\left(\frac{\dot{\gamma}_c^r}{\dot{\gamma}_o}\right)^{-1/n}\rho_c\dot{\gamma}_c^r$$

$$\dot{\rho}_{ws} = \beta^* \frac{\sqrt{3}(1-f)}{fb}\sqrt{\rho_{ws} + \rho_{wg}}\,\dot{\gamma}_c^r + (1-\xi)\beta^* \frac{6(1-f)^{2/3}}{bdf}\dot{\gamma}_c^r \quad - k_o\left(\frac{\dot{\gamma}_w^r}{\dot{\gamma}_o}\right)^{-1/n}\rho_{ws}\dot{\gamma}_w^r$$

$$\dot{\rho}_{wg} = \xi\beta^* \frac{6(1-f)^{2/3}}{bdf}\dot{\gamma}_c^r$$

$$f = f_\infty + (f_o - f_\infty)e^{(-\gamma^r/\bar{\gamma}^r)}$$

$$\rho_{tot} = f(\rho_{ws} + \rho_{wg}) + (1-f)\rho_c$$

$$d = \frac{K}{\sqrt{\rho_{tot}}}$$

Constitutive Equations for Stage II Through Stage IV:

Beyond the critical strain, we have the flow behaviour controlled by the Z parameter. The flow stress in this region is given as

$$\sigma = \sigma_P - (\sigma_P - \sigma_{ss}) * (1 - e^{-K(\frac{\varepsilon - \varepsilon c}{\varepsilon p})^n})$$

Where, $\sigma_{DRV}, \sigma_P, \sigma_{ss}, K = f(Z)$ and $X = (1 - e^{-K(\frac{\varepsilon - \varepsilon c}{\varepsilon p})^n})$

IMPLEMENTATION OF THE MATERIAL MODEL IN ABAQUS

User material subroutine VUHARD was used in Abaqus^{TM} to implement the grain refinement and coarsening during the recrystallization process.

The user material subroutine requires 4 parameters: Array containing the yield stress (for isotropic plasticity) or yield surface size (for combined hardening) at the material points, the derivative of the yield stress or yield surface size with respect to the equivalent plastic strain at the material points, the derivative of the yield stress with respect to the equivalent plastic strain rate at the material points and containing the derivative of the yield stress or yield surface size with respect to temperature at the material points.

The grain size and dislocation density are evaluated as solution dependent state variables and the resultant is stored in an array and passed into Output Requests for viewing.

The subroutine returns the value of the equivalent plastic strain at the beginning of the increment. The equivalent plastic strain rate and temperature are also available. These are used to evaluate the critical strain at that point and it is checked whether the material has crossed stage I, if so the flow stress and the other output parameters are accordingly varied.

The user-hardening subroutine is attached at the end of the file for reference.

RELEVANT RESULTS AND DISCUSSION

The user material subroutine was benchmarked against a tensile model (material-AA1200) to ensure proper conformance. The model and resulting stress-strain curve are shown.

For AA1200, the phenomenological model is the Johnson-Crook model (ref 6):

$$\sigma = (A + B * \varepsilon^{n}) * \left(1 + C * \ln\left(\frac{\dot{\varepsilon}}{\dot{\varepsilon}^{0}}\right)\right) * \left(1 - \left(\frac{(T - Tref)}{(Tm - Tref)}\right)^{m}\right)$$

The material constants taken from Ref7 are shown below:

Table 3
Johnson-Cook model parameters of commercially pure titanium and aluminum.

Material	A_{al} (MPa)	B_{al} (MPa)	n_{al}	C_{al}	m_{al}	T_{ref} (°C)	T_m (°C)	$\dot{\varepsilon}_o$ (s^{-1})
AA 1200	80	120	0.73	0.008	1.7	25	660	1
Material	B_{ti} (MPa)	n_{ti}	C_{ti}	α_{ti}	β_{ti}	T_{ref} (°C)	T_m (°C)	$\dot{\gamma}_o$ (s^{-1})
CP Ti	294.15	0.294	0.053	0.021	3.862	150	1668	0.192

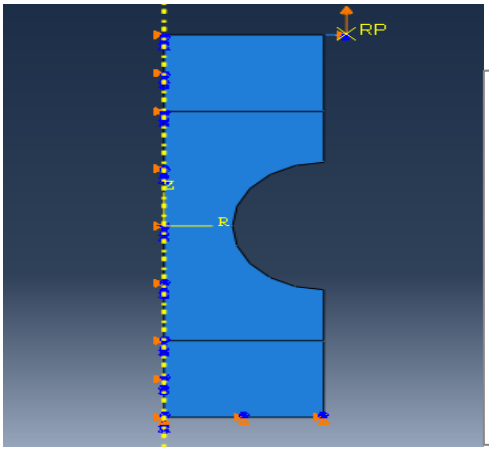

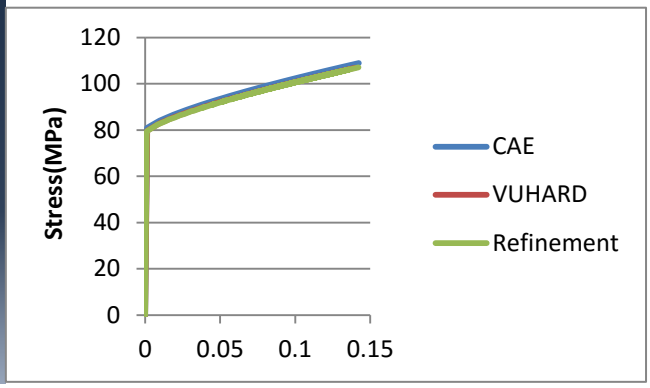

Fig. 4 -tensile test model Fig.5 – Comparison of stress/strain curves

As shown in Fig.5, the Stress is in the Y-axis(in MPa) and strain is in the X-axis. There is close conformance between the input from the CAE and input from the VUHARD as well as the dislocation density based material model (noted by "Refinement").

Then, multi-pass cold rolling was conducted using spherical rigid roller. Grain size refinement of CP Ti during the 5-pass cold rolling process was simulated with the developed multi-step Lagrangian type FE model and the dislocation material subroutine of CP Ti. Fig. 6 shows the predicted deformation and dislocation fields during the third pass cold rolling of CP Ti in terms of (a) equivalent strain, (b) total dislocation density and (c) grain size. Significant strain gradients can be observed not only in the roll-workpiece contact area but also in the normal direction of the steady-state rolled part. Dislocations accumulate more as strain increases, as can be seen in Fig. 6(b), which shows a similar pattern to the strain.

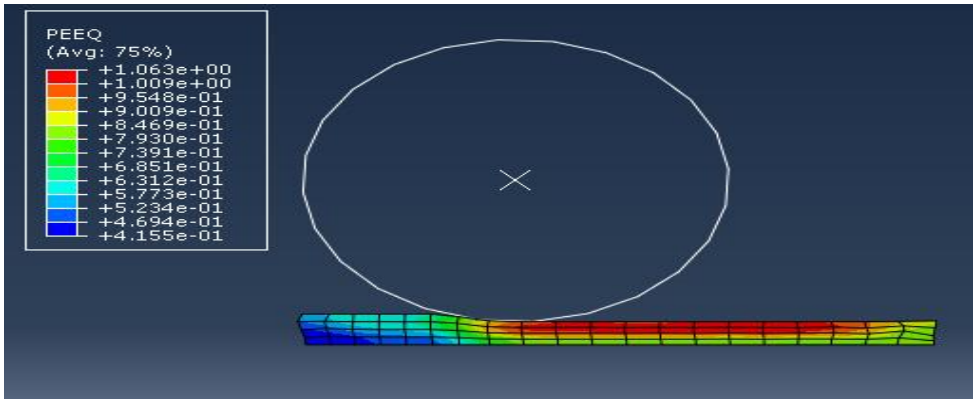

Fig. 6(a)- Equivalent plastic strain

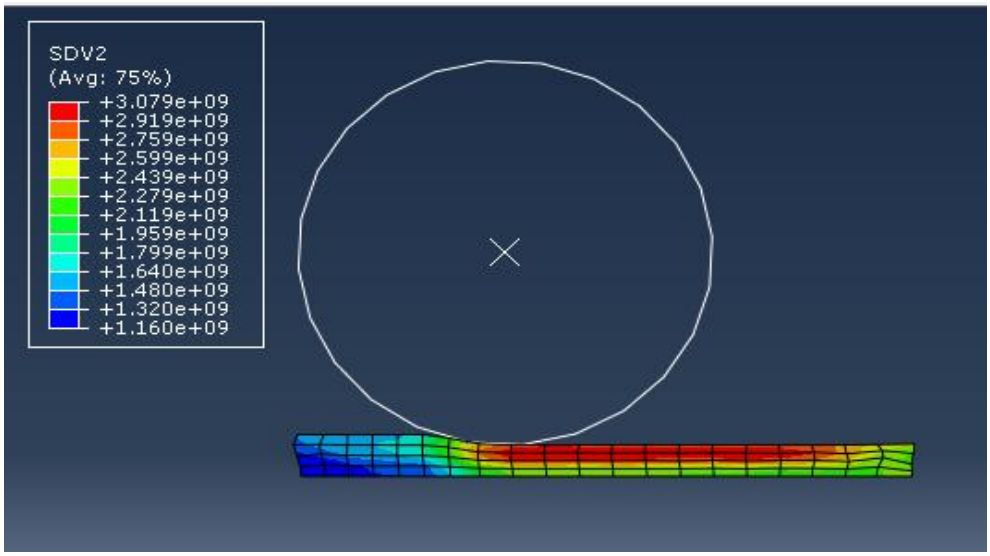

Fig 6(b) – Dislocation density

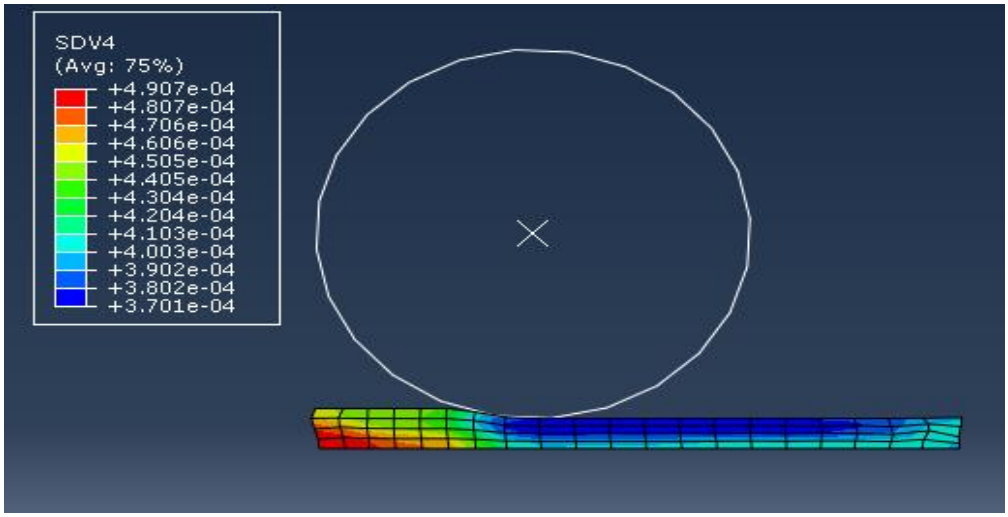

Fig 6(c)- Grain size

The plot in Fig.7 shows the comparison between the grain sizes obtained by the grain refinement and measured values.

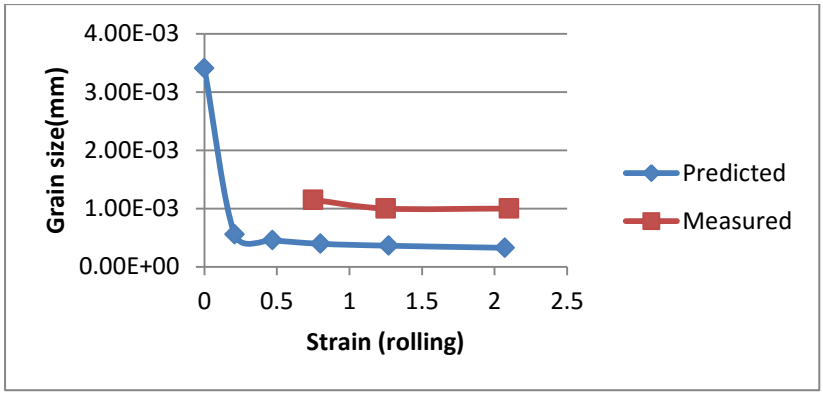

Fig.7

Noting the distinction between the two, we can conclude that recrystallization has occurred at larger plastic strains here, and the grain size which in turn depends on the yield stress has not shown significant decrease after a certain strain, indicating that steady state stress has been reached.

The recrystallization material model was also implemented with VUHARD subroutine in the tensile model shown above.

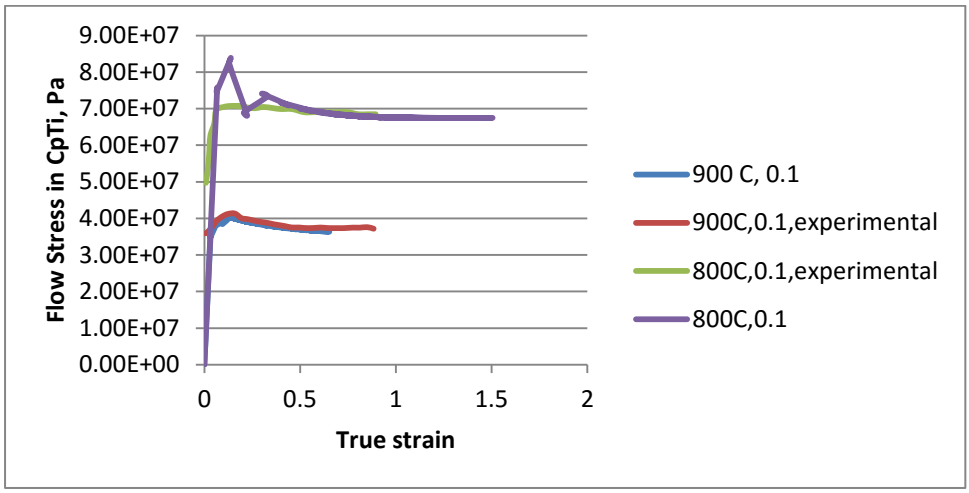

Fig.8 – Stress/strain curve taking recrystallization into consideration

The tensile test was done isothermally at two different temperatures, 800^{o} C and 900^{o}C. The strain rates in both cases were the same (ie) 0.1s^{-1}. The plot shows comparison between the two results. It is clear that the flow stress is reasonably predicted.

The next step is to implement the above model for multi pass cold rolling. It is not immediately clear what to use as a strain rate for the non-isothermal process. Two types of averages have been proposed: the strain and time-average.

$$\bar{\varepsilon}(rate)_{strain-average} = (\overline{\varepsilon} * \Delta\varepsilon)/\dot{\varepsilon}_{avg}$$

And a similar time-average can be determined. The jumps from one strain rate to another, as is happens between two different passes of the rolling process is seamless with perhaps only a small transient as illustrated by Fig. 9

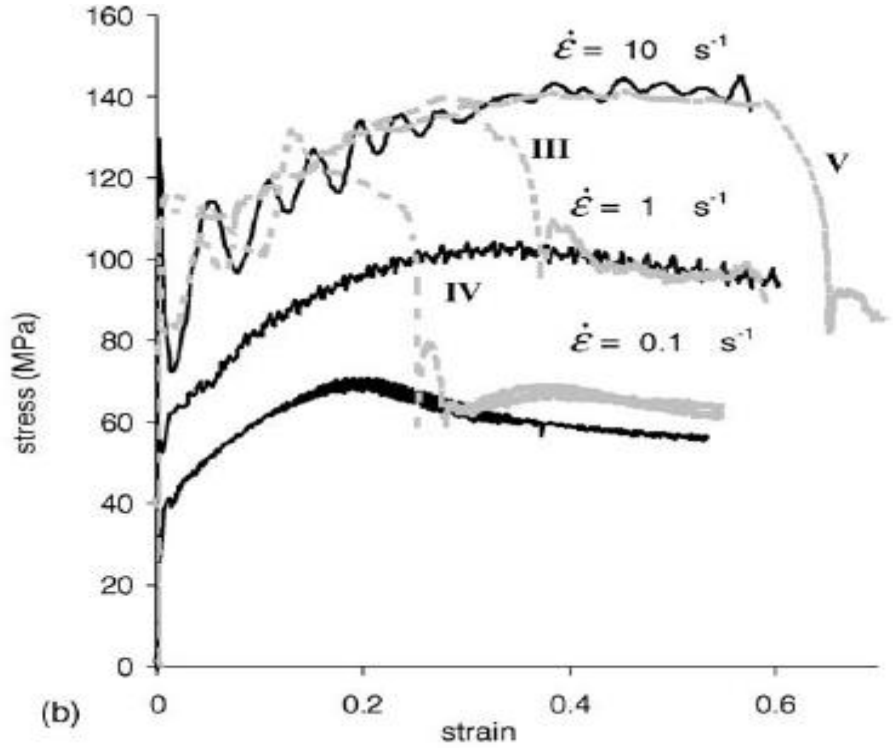

Fig.9 (from ref11) – showing sudden jumps from one strain rate to another(in grey)

Hence, this method needs to be used for implementing multi-pass cold rolling to predict the grain coarsening as a function of the strain and process parameters.

CONCLUSION:

Hence, the user material subroutine developed in ABAQUS has been used to test the flow behaviour of metals in hot working conditions and it will later be used to implement multi pass cold rolling for prediction of grain size.

REFERENCES

1. Liu, Q., Huang, X., Lloyd, D.J., Hansen, N., 2002. Microstructure and strength of commercial purity aluminium (AA 1200) cold-rolled to large strains. *Acta Materialia 50, 3789‑3802.*
2. Yang, D.K., Cizek, P., Hodgson, P.D., Wen, C.E., 2010. Microstructure evolution and nanograin formation during shear localization in cold-rolled titanium. *Acta Materialia 58, 4536–4548.*
3. M. Shaban, B. Eghbali, Determination of critical conditions for dynamic recrystallization of a microalloyed steel, *Materials Science and Engineering: A, Volume 527, Issues 16–17, 25 June 2010, Pages 4320-4325, ISSN 0921-5093, http://dx.doi.org/10.1016/j.msea.2010.03.086.* (http://www.sciencedirect.com/science/article/pii/S0921509310003606)
4. Sheikh-Ahmad, J.Y., Bailey, J.A., 1995. A constitutive model for commercially pure titanium. *Transactions of the ASME. Journal of Engineering Materials and technology117, 139‑144.*
5. Akbari Mousavi, S.A.A., Ranjbar Bahadori, S., Shahab, A.R., 2010. Numerical and experimental studies of the plastic strains distribution using subsequent direct extrusion after three twist extrusion passes. *Materials Science and Engineering A 527, 3967–3974.*
6. Johnson, G.R.; Cook, W.H. (1983), "A constitutive model and data for metals subjected to large strains, high strain rates and high" , *Proceedings of the 7th International Symposium on Ballistics*: 541–547
7. Hongtao Ding, Ninggang Shen, Yung C. Shin, Predictive modeling of grain refinement during multi-pass cold rolling, *Journal of Materials Processing Technology, Volume 212, Issue 5, May 2012, Pages 1003-1013, ISSN 0924-0136, http://dx.doi.org/10.1016/j.jmatp*
8. Vincent Lemiale, Yuri Estrin, Hyoung Seop Kim, Robert O'Donnell, Grain refinement under high strain rate impact: A numerical approach, *Computational Materials Science, Volume 48, Issue 1, March 2010, Pages 124-132, ISSN 0927-0256, http://dx.doi.org/10.1016/j.commatsci.2009.12.018.* (http://www.sciencedirect.com/science/article/pii/S0927025609004765)
9. Estrin, Y., Toth, L.S., Brechet, Y., Kim, H.S., 2006. Modelling of the evolution of dislocation cell misorientation under severe plastic deformation. *In: 3rd International Conference on Nanomaterials by Severe Plastics Deformation, NanoSPD3, September 22, 2005‑September 26, 2005. Trans Tech Publications Ltd., Fukuoka, Japan, pp. 675‑680.*
10. Abaqus documentation, version 6.12- "*https://things.maths.cam.ac.uk/computing/software/abaqus_docs/docs/v6.12/index.html*"
11. Modelling of DRX and MDRX during bar rolling of a medium carbon spring steel.